

Asymmetries for elastic scattering of π^\pm from polarized ^3He at Δ resonance energies

M. A. Espy,* J. M. O'Donnell, B. Davis, D. Dehnhard, J. L. Langenbrunner,* B. Larson, M. Palarczyk,† C. M. Riedel,* and K. Wick

School of Physics and Astronomy, University of Minnesota, Minneapolis, Minnesota 55455

S. Blanchard, G. R. Burleson, W. R. Gibbs, B. Lail, B. Nelson, B. K. Park,* and Q. Zhao‡

Department of Physics, New Mexico State University, Las Cruces, New Mexico 88003

W. J. Cummings,§ P. P. J. Delheij, B. K. Jennings, O. Häusser, R. Henderson, and D. Thiessen

TRIUMF, Vancouver, Canada V6T 2A3

E. Brash|| and M. K. Jones¶

Department of Physics, Rutgers University, Piscataway, New Jersey 08854

B. Brinkmüller**

Institut für Experimentelle Kernphysik der Universität Karlsruhe, Karlsruhe, Germany

K. Maeda

Department of Physics, Tohoku University, Kawachi, Sendai, Japan

F. Merrill, C. L. Morris, S. Penttilä, D. Swenson,†† and D. Tupa

Los Alamos National Laboratory, Los Alamos, New Mexico 87545

C. Bennhold

Department of Physics, Center for Nuclear Studies, The George Washington University, Washington, D.C. 20052

S. S. Kamalov

Laboratory of Theoretical Physics, JINR, 141980 Dubna, Moscow Region, Russia

(Received 4 August 1997)

Asymmetries A_y for π^+ and π^- elastic scattering from polarized ^3He were measured at incident energies passing through the π nucleon P_{33} , or $\Delta(1232)$, resonance. The data were taken at the Clinton P. Anderson Meson Physics Facility using the high-energy pion channel P^3 and a large acceptance spectrometer to detect the scattered pions. The polarized ^3He target, originally developed at TRIUMF, was modified for these experiments by the addition of diode lasers. Completely unexpected negative asymmetries were observed at and below the resonance in π^+ scattering near 50° – 60° , which cannot be reproduced by multiple scattering theory and Faddeev wave functions. A hybrid model, which adds a Δ -neutron spin-spin interaction term to the conventional calculations, provides a good description of the π^+ data. For π^- scattering this term predicts a negligible effect on A_y and the data do not show the anomalous A_y seen with π^+ . [S0556-2813(97)05611-2]

PACS number(s): 25.80.Dj, 25.10.+s, 24.70.+s

*Present address: Los Alamos National Laboratory, Los Alamos, NM 87545.

†Present address: Department of Physics, Ohio State University, Athens, OH 45701.

‡Present address: Radiation Oncology, University of Michigan, Ann Arbor, MI 48109.

§Present address: Argonne National Laboratory, Argonne, IL 60439.

||Present address: Department of Physics, University of Regina, Regina, SK, Canada S4S 0A2.

¶Present address: College of William & Mary, Williamsburg, VA 23187.

**Present address: SAP-AG, Karlsruhe, Germany.

††Present address: Varian Ion Implant Systems, Gloucester, MA 01930.

I. INTRODUCTION

In a recent Letter [1] we reported preliminary results of asymmetry measurements in π^+ elastic scattering from polarized ^3He at incident energies passing through the π -nucleon P_{33} , or $\Delta(1232)$, resonance. This paper presents a detailed description of the experiment and the theoretical analysis of the final results for π^+ scattering and of data for π^- scattering taken recently.

Pion elastic scattering asymmetries depend sensitively on the spin-dependent parts of the π -nucleus interaction, whereas differential cross sections depend primarily on the spin-independent parts. Measurements of elastic asymmetries thus provide information on the spin dependence of the π -nucleus reaction mechanism and the target ground-state

density. In the late 1980s it had become possible [2] to achieve significant nuclear polarizations for targets of $1p$ -shell nuclei of spin $\frac{1}{2}$. Elastic scattering asymmetries measured with these targets were found to be in disagreement with theoretical predictions that used a first-order optical potential and shell-model wave functions. For example, experiments on ^{15}N [3,4] and ^{13}C [5–8] measured generally small values of A_y , whereas theory predicted [9–11] that A_y should be large at some angles.

The theoretical A_y for elastic scattering from $1p$ -shell nuclei show a strong dependence [6,7,11] on the details of the nuclear structure, implying that information on the spin-dependent part of the nuclear ground-state density is contained in the data. Thus the failure of theory to reproduce the measured A_y indicates that either the π -nucleus reaction mechanism and specifically its spin dependence is not yet understood or that the nuclear wave functions of these nuclei are not sufficiently well known, or both.

One way to proceed was to conduct a polarization experiment on a nucleus of well-known nuclear structure such as ^3He , which is a much simpler nucleus than the $1p$ -shell nuclei used in the previous experiments. Reliable wave functions have been obtained by Faddeev calculations [12–14] so that spin-dependent effects in the π -nucleus interaction can be studied without large uncertainties in the nuclear structure.

Such experiments became possible in the early 1990s with the development of a high-density, optically pumped ^3He gas target at TRIUMF [15]. This target was used at TRIUMF for the measurement of A_y for π^+ scattering from polarized ^3He at an incident pion energy $T_\pi=100$ MeV [16]. π^- data at this energy were also subsequently taken [17]. At this energy, theory predicts [18] for both π^+ and π^- scattering that the asymmetry is insensitive to the nuclear wave function and shows only a slight dependence on the reaction model. However, for energies at and above the $\Delta(1232)$ resonance, the asymmetries are predicted to become increasingly sensitive to the details of the reaction model. Thus there was considerable interest in an extension of these measurements to energies at and above the P_{33} resonance.

The $P^3\text{East}$ beamline at Clinton P. Anderson Meson Physics Facility (LAMPF) provided superior beam flux at energies at and above the P_{33} resonance than could be achieved at TRIUMF. In addition, LAMPF had a spectrometer suitable for the Δ resonance energies. Thus the TRIUMF target was moved and the asymmetry measurements reported here, π^+ and π^- scattering on polarized ^3He through the Δ resonance region, were performed at LAMPF.

The data for π^+ and π^- were taken in two separate experiments. The A_y for π^+ scattering, measured first [1], were found to exhibit some unexpected characteristics. Most surprisingly, at $T_\pi=142$ and 180 MeV and angles near 50° – 60° , the A_y were found to be fairly large and negative (≈ -0.30). This result was in contradiction to all conventional model calculations at that time [18–20], which predicted small positive asymmetries. Near 80° the experimental A_y were large and positive, but the maximum was shifted to higher angles than predicted. As discussed in the Letter [1] and in more detail in this paper, the anomalous angular distribution of A_y for π^+ scattering at 180 MeV can be fit very well by a hybrid model developed by one of us (B.K.J.). This

model uses the first-order multiple-scattering amplitudes of Ref. [18], but adds a second-order term to the spin-dependent amplitude that accounts for a Δ -neutron spin-spin interaction (DINT). For π^+ scattering this second-order term is comparable to the first-order term owing to the different isospin couplings for π^+p and π^+n . This model predicts that the DINT term for π^- scattering is much smaller relative to the first-order terms. Thus the effects of DINT on the A_y for π^- ^3He should be negligible. Indeed, π^- data taken recently [21] and presented in this paper as well are described equally well by calculations that do or do not include a DINT term.

Section II summarizes briefly the formalism of pion scattering from a polarized spin- $\frac{1}{2}$ target. Section III describes the experiments, Sec. IV discusses the extraction of the experimental asymmetries and their uncertainties, and Sec. V presents a theoretical analysis of the data using several different models. Section VI concludes briefly.

II. PION ELASTIC SCATTERING ON POLARIZED SPIN- $\frac{1}{2}$ NUCLEI

The amplitude [22] $F(\theta, \phi)$, for scattering of a spin-0 particle, like the pion, from a spin-1/2 nucleus has a spin-independent (\mathcal{F}) and a spin-dependent (\mathcal{G}) part,

$$F(\theta, \phi) = \mathcal{F}(\theta) + i\mathcal{G}(\theta)\hat{n} \cdot \vec{\sigma}, \quad (1)$$

where $\vec{\sigma}$ are the nuclear Pauli spin matrices and \hat{n} , the normal to the reaction plane, is defined by the incident and scattered particle's momentum vectors \vec{k}_i and \vec{k}_f , respectively,

$$\hat{n} = \frac{\vec{k}_i \times \vec{k}_f}{|\vec{k}_i \times \vec{k}_f|}. \quad (2)$$

The spin-dependent amplitude $\mathcal{G}(\theta)$, often called the spin-flip amplitude, involves one unit of spin transfer to the target ($\Delta S=1$), whereas the spin-independent amplitude $\mathcal{F}(\theta)$ proceeds without spin transfer ($\Delta S=0$). Both $\mathcal{F}(\theta)$ and $\mathcal{G}(\theta)$ have isoscalar ($\Delta T=0$) and isovector ($\Delta T=1$) parts.

Since the pion has no spin, the only spin-dependent interaction in *pion-nucleon* scattering is the spin-orbit force involving the nucleon's spin and the relative angular momentum of the pion and nucleon. The spin-dependent amplitude for *pion-nucleus* elastic scattering $\mathcal{G}(\theta)$ involves the *pion-nucleon* elastic scattering amplitude, the spin-dependent part of the nuclear ground-state density, and possible second-order effects resulting, for example, from the spin-dependent interaction of the intermediate $\Delta(1232)$ with the nuclear core.

The only spin-dependent observable presently accessible for spin- $\frac{1}{2}$ nuclei is the analyzing power (or left-right scattering asymmetry) A_y . In asymmetry experiments, rather than move the spectrometer from right to left of the beam, the spin of the target is alternated between ‘‘up’’ (spin parallel to the normal of the reaction plane) and ‘‘down’’ (spin antiparallel to the normal of the reaction plane).

For a target with polarizations $P_{up} = P_\uparrow$ and $P_{down} = P_\downarrow$ the differential cross sections with spin up and down, respectively, are [22]

$$\frac{d\sigma}{d\Omega}_\uparrow = |\mathcal{F}(\theta)|^2 + |\mathcal{G}(\theta)|^2 + 2P_\uparrow [\text{Im}\mathcal{F}(\theta)\text{Re}\mathcal{G}(\theta) - \text{Im}\mathcal{G}(\theta)\text{Re}\mathcal{F}(\theta)] \quad (3)$$

and

$$\frac{d\sigma}{d\Omega}_\downarrow = |\mathcal{F}(\theta)|^2 + |\mathcal{G}(\theta)|^2 - 2P_\downarrow [\text{Im}\mathcal{F}(\theta)\text{Re}\mathcal{G}(\theta) - \text{Im}\mathcal{G}(\theta)\text{Re}\mathcal{F}(\theta)]. \quad (4)$$

Thus

$$\frac{d\sigma}{d\Omega} = |\mathcal{F}(\theta)|^2 + |\mathcal{G}(\theta)|^2 \quad (5)$$

and

$$A_y = \frac{\frac{d\sigma}{d\Omega}_\uparrow - \frac{d\sigma}{d\Omega}_\downarrow}{P_\downarrow \frac{d\sigma}{d\Omega}_\uparrow + P_\uparrow \frac{d\sigma}{d\Omega}_\downarrow} = \frac{2 \text{Im}[\mathcal{F}(\theta) \mathcal{G}(\theta)^*]}{|\mathcal{F}(\theta)|^2 + |\mathcal{G}(\theta)|^2}, \quad (6)$$

$$= \frac{2 \text{Im}[\mathcal{F}(\theta) \mathcal{G}(\theta)^*]}{|\mathcal{F}(\theta)|^2 + |\mathcal{G}(\theta)|^2}, \quad (7)$$

i.e., A_y is due to the interference between the spin-dependent and spin-independent amplitudes. A measurement of A_y is a sensitive way to probe the small spin-dependent amplitude \mathcal{G} and the phase between \mathcal{F} and \mathcal{G} . Whereas cross sections are proportional to the sum of the amplitudes squared and are generally dominated by $|\mathcal{F}(\theta)|^2$, the asymmetry is strongly sensitive to both amplitudes. If the amplitudes \mathcal{F} and \mathcal{G} are comparable in magnitude (as near the minima in the cross section) and their relative phase is near 90° or 270° , the asymmetry can be as large as ± 1.0 .

A simple model (toy model) of π - ^3He elastic scattering has been constructed assuming that the ground state (g.s.) of ^3He consists entirely of the space-symmetric S state [18]. In this model the π - ^3He elastic scattering amplitudes are given by

$$\mathcal{F} = (2f_{\pi p} + f_{\pi n})F_0(Q^2), \quad (8)$$

$$\mathcal{G} = g_{\pi n}F_1(Q^2), \quad (9)$$

where $f_{\pi N}$ and $g_{\pi N}$ are the free πN spin-independent and spin-dependent amplitudes and F_0 and F_1 are, respectively, the spin-independent and spin-dependent nuclear form factors. In \mathcal{F} the contributions from the two protons and the neutron add coherently. However, since the spins of the protons are coupled to zero, the only contribution to \mathcal{G} is from the unpaired neutron. The ^3He form factors were assumed to be spin independent and to have a Gaussian shape

$$F_0(Q^2) = F_1(Q^2) = \exp\left(-\frac{1}{6}r_0^2Q^2\right). \quad (10)$$

Here $r_0 = 1.65$ fm is the rms radius of the distribution of nucleon centroids in ^3He . Q^2 , the square of the three-

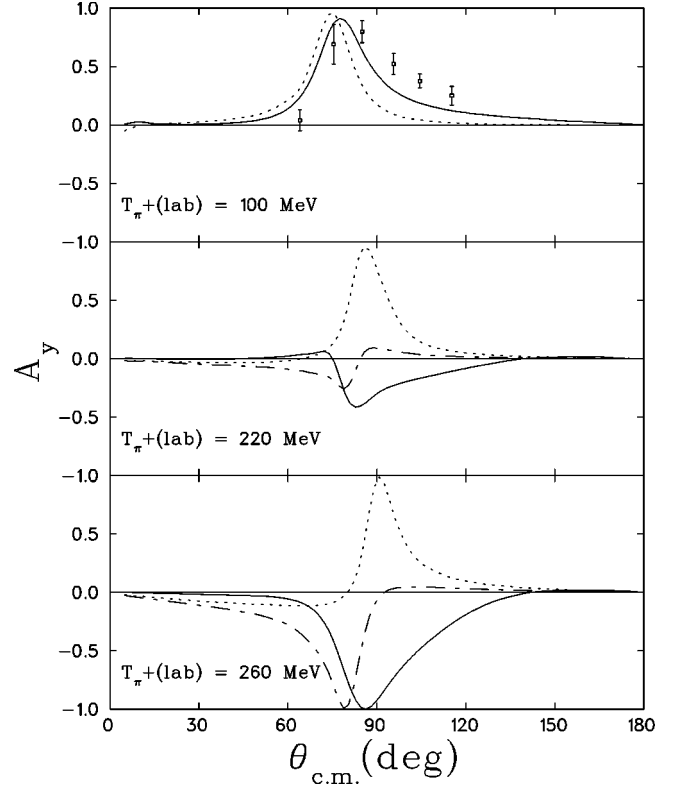


FIG. 1. Asymmetries for π^+ elastic scattering from ^3He at 100, 220, and 260 MeV. The data at 100 MeV (top panel) are from Ref. [17]. The solid curves show the full KTB calculations [18] and the dotted lines were obtained with the toy model (see the text). The chain-dashed curves are from the toy model with the modification for multiple scattering [Eq. (11)] with $A=0.4$ and 0.6 for 220 (middle panel) and 260 MeV (bottom panel), respectively.

momentum transfer, equals $4q_i^2\sin^2(\theta/2)$ and q_i is the incident pion momentum in the center of mass and θ the scattering angle in the center of mass. Multiple-scattering effects (which are predicted to become important at energies above the P_{33} resonance) are simulated in this model by modifying [18] the real part of \mathcal{F} by the addition of a term proportional to $F_0(Q^2)$, that is,

$$\text{Re}\mathcal{F} \rightarrow \text{Re}\mathcal{F} + AF_0(Q^2). \quad (11)$$

A is a real number that does not depend on angle, but may depend on the pion energy.

Initial asymmetry measurements for elastic π - ^3He scattering, done at TRIUMF at $T_\pi = 100$ MeV [15–17], obtained values of A_y that were large and positive with a maximum of nearly $+1$ around $\theta_{cm} = 90^\circ$. (See the top panel of Fig. 1 for π^+ data and predictions at 100 MeV.) This was in contrast to the small asymmetries observed for the $1p$ -shell nuclei.

The large asymmetry for π^+ elastic scattering from ^3He is, at first, surprising as the elementary A_y for π^+ -neutron scattering is rather small [23]. However, as described above, A_y depends sensitively on the magnitudes of and relative phase between \mathcal{F} and \mathcal{G} . \mathcal{F} for scattering, from ^3He involves both protons and the neutron and is thus quite different from f for π -neutron scattering whereas \mathcal{G} is due to the neutron only as in the free π -neutron case.

The 100-MeV ^3He data for π^+ (Fig. 1, top panel) (and π^- , not shown) are described quite well (dotted lines) by the toy model without the modification of Eq. (11) for multiple scattering, which has only a small effect at this energy. The data are also well described (solid lines) by the model developed by Kamalov, Tiator, and Bennhold [18]. This model is based on the Kerman-McManus-Thaler formulation of multiple-scattering theory [24]. The Kamalov-Tiator-Bennhold (KTB) model uses a microscopic description of the pion-nuclear interaction in momentum space, the coupled-channel method, realistic free π - N scattering amplitudes, and the Faddeev wave function for ^3He .

The predictions for asymmetries for π^- at 100 MeV are also independent of the model. However, at energies above the centroid of the P_{33} resonance (220 and 260 MeV) the theoretical curves for π^+ and π^- display an increasing sensitivity of the asymmetries to the details of the scattering model [18]. This is highlighted in the middle and bottom panels of Fig. 1 by the different signs of A_y for π^+ scattering at 80° predicted by the three models: the toy model without and with the modification (chain-dashed lines) of Eq. (11) and the KTB model. The KTB and the toy model, if modified for multiple scattering at 220 and 260 MeV, predict the A_y at 80° to flip from positive to negative as the incident energy passes through the P_{33} resonance. The unmodified toy model predicts that the A_y stays positive between 100 and 260 MeV. The predictions of increasing sensitivity (with increasing energy) of the A_y to the scattering model and the relative insensitivity to the nuclear wave function motivated the experiments described in this paper.

III. EXPERIMENTS

Two separate experiments E1317 and E1267, were done using the high-energy pion channel, P³East, at LAMPF. During E1267, the A_y were measured for π^+ elastic scattering at $T_\pi=142, 180,$ and 256 MeV. The A_y for π^- elastic scattering were measured at 180 MeV in E1317. The polarized ^3He target apparatus was a modified version of the high-density, optically pumped system developed at TRIUMF [15]. Modifications to the target, implemented for E1267 and E1317, are discussed below and in Ref. [25].

A. Polarized ^3He target

The principle of polarizing ^3He nuclei is to first optically pump the $D1$ (794.7 nm) transition in Rb vapor, which results in the polarization of the spin of the valence electron. This polarization is then transferred to the ^3He nuclear spin by a contact hyperfine interaction between the Rb electron and the ^3He nucleus, which occurs during Rb- ^3He collisions. A 3-mT uniform holding field at the target was supplied by the horizontally mounted Helmholtz coils (Fig. 2).

The ^3He target cells were made of quartz glass. They were cylindrical in shape, of 4.5 cm inner diameter, about 6.5 cm in total length, with roughly hemispherical end caps (Fig. 3). The glass was ≈ 1.5 mm thick at the cell's cylindrical walls and 0.4 mm thick at the end caps (where the pion beam entered and exited the cell). Two cells were used during the course of the experiments, both of the same geometry. Target cells were filled with 5–7 atm of ^3He gas, a

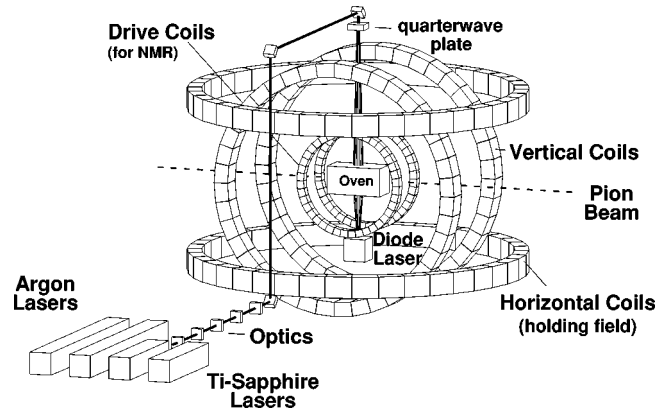


FIG. 2. TRIUMF polarized ^3He target as modified for E1267.

trace of Rb, and a small amount (about 100 torr) of N_2 to assist in the optical pumping. The wall relaxation times [15] for these cells were approximately 20 h.

Target cells were placed in an oven made of Vespel, with Kapton windows, and were heated to $\approx 180^\circ\text{C}$ to achieve the desired gaseous rubidium number density. When the cells were hot, small amounts of ^3He leaked out. The leaking resulted in an exponential decrease in the pressure with time constants of 1500 and 3500 h for the two cells used during the experiments. The leak rate at room temperature was found to be 15 times slower and thus negligible. In order to correct for the loss in target pressure, we kept track of the times that the cells were hot and the cells' temperature. We also did periodic measurements of the cells' pressures.

The laser system for E1267 consisted originally of two titanium-sapphire lasers each being pumped by one argon laser. A diode laser was added later, after one of the argon lasers began to deteriorate. With the laser and optical configuration shown in Fig. 2, we managed to keep about 8 W of circularly polarized $D1$ light on the target through the experiment. During E1317 the laser system was further modified to use only diode lasers. During E1267 the ^3He polarizations were ≈ 35 – 45% , once reaching as high as 50%. Polarizations during E1317 were typically 35%.

During both experiments, the helicity of the laser light was changed by a computer-controlled change of the orien-

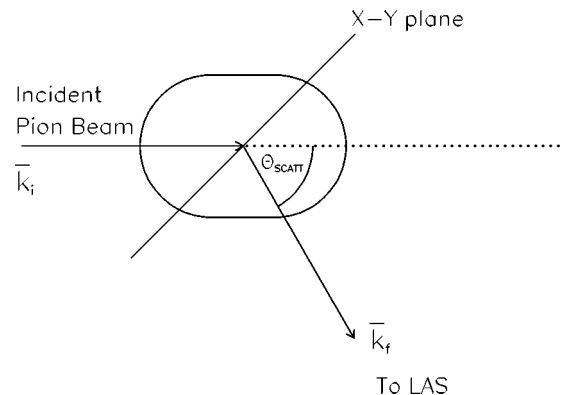


FIG. 3. Cross section of the ^3He target cell in the reaction plane. Θ_{scatt} is the scattering angle; normal to the reaction plane is into the page (+y axis of right-handed coordinate system) and the momentum vector of the scattered pion \vec{k}_f is pointing along the z axis. The x-y plane is indicated at $z=0$.

tation of a quarter-wave plate that converted linearly polarized laser light to either left-hand or right-hand circularly polarized light. In E1267 the helicity of the light (and thus the signs of the target polarization and the asymmetry) was determined by use of a liquid crystal that transmitted only light of left-hand polarization. During E1317 a system of analyzers, polarizers, and quarter-wave plates was used to determine the helicity.

The polarization of the ^3He was reversed every 11 min in order to minimize systematic errors. This was done by turning down the vertical holding field, provided by the horizontally mounted Helmholtz coils while ramping up a horizontal holding field, provided by the vertically mounted Helmholtz coils (Fig. 2). Then the vertical holding field was ramped up in the reverse direction while the horizontal holding field was returned to zero. The entire procedure took about 19 sec. No data were taken during the polarization reversal. The NMR apparatus was calibrated by measurement of the small signal from protons in a water-filled cell of approximately the same dimensions. The protons in the water-filled cell were polarized by the small holding field.

B. Pion beam

The pion beam of the high-energy pion channel at LAMPF, P³East, was used. An achromatic beam tune was employed that provides a narrow waist at the center of the target cell thus preventing most of the beam from hitting the target cylindrical cell walls (Fig. 3). However, use of the achromatic tune caused the overall energy resolution of the experiment to be limited to about 4 MeV [full width at half maximum (FWHM)] owing to the momentum spread in the incident beam. The size of the beam spot at the target was roughly $2.2 \times 2.2 \text{ cm}^2$, with an estimated 98% of the beam intercepting this area. The divergence of the beam at the target was about 44 mrad horizontally and 22 mrad vertically. In order to reduce the amount of beam halo ($\approx 2\%$ of the beam) that might strike the target cell walls and produce background, a lead collimator was placed upstream of the target. This collimator was machined by a computer driven lathe to match the beam divergence and proved to be quite effective.

An ion chamber (IC) at the end of the P³East beam pipe monitored the beam flux entering the target cave. The IC was used for all relative normalizations between spin states to account for possible differences in the number of pions between spin-up and spin-down measurements. No attempt was made to measure absolute differential cross sections. Typical pion fluxes for both experiments were between $2 \times 10^7 \pi/\text{sec}$ and $10^8 \pi/\text{sec}$ depending on a variety of factors such as beam polarity, beam energy, jaw settings, and proton current on the pion production target.

C. Large acceptance spectrometer

The large acceptance spectrometer (LAS), a quadrupole-quadrupole-dipole system, was used to momentum analyze the scattered pions. A detailed description of the LAS can be found in Refs. [26,27]. The momentum acceptance $\Delta p/p$ of the LAS was about 5% in both E1267 and E1317 and the solid angle was approximately 15 msr. The LAS contribution of 1 MeV to the energy resolution width was negligible com-

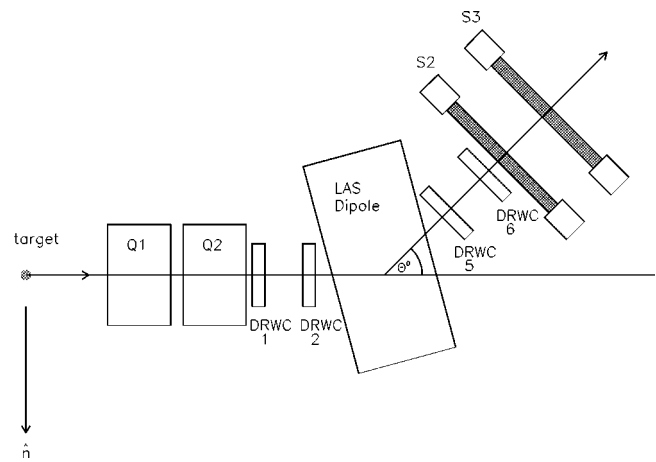


FIG. 4. Layout of the large acceptance spectrometer (LAS).

pared to the contribution from the momentum spread in the beam. Some modifications have been made to the spectrometer since the original design. A side view of the LAS spectrometer as it was used in E1267/E1317 is presented in Fig. 4.

The spectrometer uses four pairs of delay-line readout drift chambers (DRWCs) [28], the first two pairs being located (see Fig. 4) between the quadrupoles and the dipole (front chambers) and the last two pairs just after the dipole (rear chambers). Each pair of chambers has two planes of wires, one stretched vertically, the other horizontally. The wire planes consist of alternating anode and field-defining cathode wires with 4-mm spacings between adjacent wires. The planes with vertically stretched wires provide the y position and dy/dz , whereas the planes with horizontally stretched wires provide the x position and dx/dz . The z axis in this coordinate system coincides with the optical axis of the quadrupole doublet, with $z=0$ at the center of the target (Fig. 3). The information on x , y , dx/dz , and dy/dz from the front and rear chambers is used to determine the trajectory of the charged particle through the spectrometer and to trace that trajectory back to the target.

Position resolution of trajectories projected back to the target was 0.4 cm (FWHM) horizontally. Such good horizontal position resolution is needed to eliminate efficiently the large number of events from the target cell end caps. Vertical resolution was not as good, but was not as crucial to this experiment as the horizontal resolution.

Since the energy resolution of the spectrometer would be affected by multiple scattering in the air between the target and the rear chambers, helium bags were installed along the 6-m flight path through the spectrometer. A helium bag was also placed between the IC and the target oven to reduce multiple scattering in air prior to the target. Located behind the rear chambers were two scintillators $S2$ and $S3$, which measured time-of-flight and energy loss for particle identification.

The coordinates $XTGT$ and $YTGT$ of the intersections of the particle trajectories with the x - y plane at $z=0$ were calculated from the wire chamber signals and the LAS calibrations. A two-dimensional histogram of events in the x - y plane, called XYT , is shown in Fig. 5. The regions of high intensity are from π scattering and reactions in the end caps, where the pion beam enters and exits the target cell (see Fig.

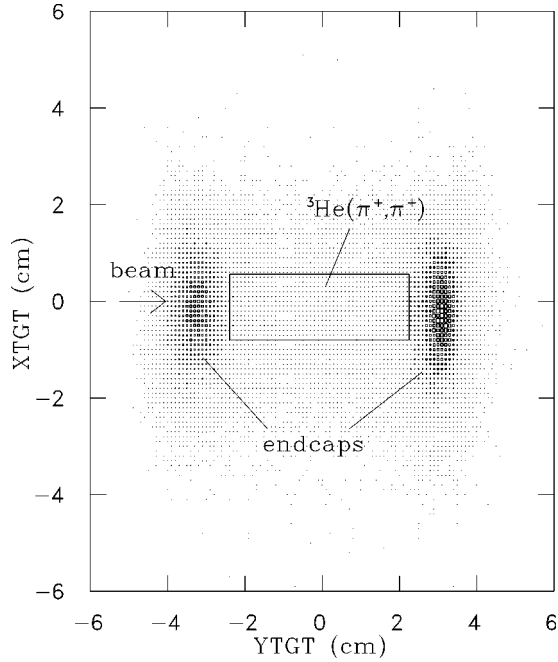


FIG. 5. Projections of the interaction vertices onto the x ($XTGT$) and y ($YTGT$) axes. This $XYTYT$ spectrum was taken at $\Theta_{scatt}=90^\circ$. Regions of high intensity are from pions scattered on the end caps of the target cell (where the pion beam enters and exits). A software cut on the “interior” region of the cell is indicated by the rectangular box.

3). Pions scattered from the ^3He gas can only come from within the cell and so a rectangular software cut was placed on this area. Note that such a cut on the cell’s interior region may contain beam particles (not intercepted by the collimator) that scattered from the sidewalls of the target.

IV. DETERMINATION OF A_y

A. Energy spectra

With the software cut on $XYTYT$, excitation energy spectra $M_\uparrow(E_x)$ and $M_\downarrow(E_x)$ were generated assuming $^3\text{He} + \pi$ kinematics so that events scattered elastically from ^3He appear at E_x (referred to as “missing mass”) = 0. Typical spin-sorted E_x (missing mass) spectra are shown in the upper and middle panels of Fig. 6. The peak from π elastic scattering on ^3He is clearly visible at $E_x=0$. The overall energy resolution is about 4 MeV (FWHM) primarily due to the large momentum spread in the incident achromatic beam. Nevertheless, this resolution width is sufficient to resolve the elastic peak from the ^3He breakup continuum ($E_x \geq 7.7$ MeV). Events from elastic scattering on silicon and oxygen (the major constituents of the quartz glass) or inelastic scattering to excited states of these nuclei, which were not eliminated by the software cut on $XYTYT$, may appear at excitations energies from $E_x \leq 0$ up to high excitation energy and may thus interfere with the elastic peak from ^3He near $E_x=0$. Therefore, background spectra were measured at many angles using empty cells. [There is so little of the buffer gas N_2 (≈ 100 torr) and Rb vapor in the target cell that background from these contaminants is negligible.]

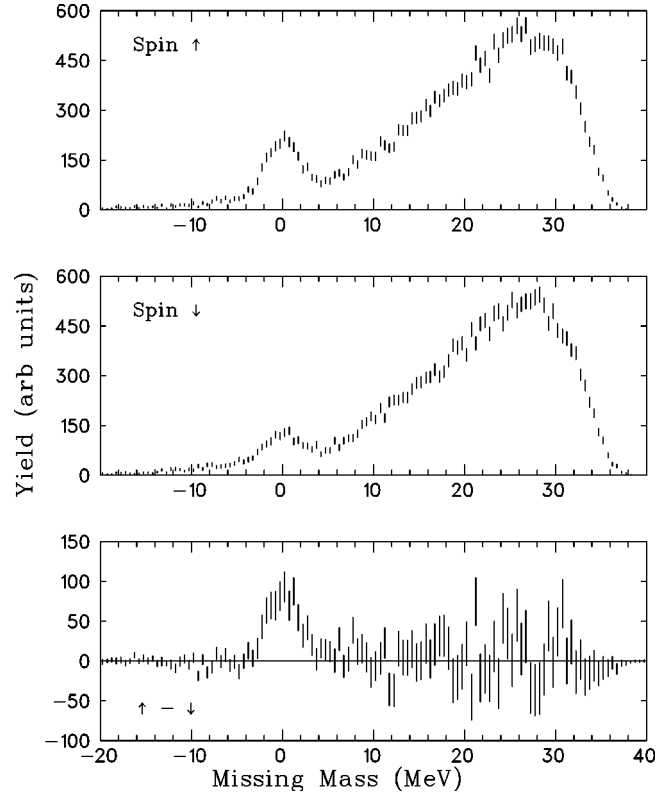


FIG. 6. Energy spectra $M(E_x)$ measured at $T_{\pi^+}=180$ MeV, $\theta_{lab}=80^\circ$. Upper panel, M_\uparrow ; middle panel, M_\downarrow ; lower panel, $M_\uparrow - M_\downarrow$. A large, positive asymmetry is apparent for the elastic scattering peak. A_y above the breakup threshold ($E_x \geq 7.7$ MeV) is consistent with zero.

B. Background spectra

The background from the glass has primarily two contributions. The first results from elastic and inelastic scattering from Si and O as the pions travel through the thin windows (≈ 0.4 mm thick) at the end caps of the cell. The elastic peaks and the yields from transitions to the 3^- states (6.13 MeV and 6.88 MeV) in ^{28}Si and ^{16}O , respectively, were found to be the most prominent. The 2^+ state in ^{28}Si at 1.77 MeV was not resolved from the ground state. The second contribution to the glass background results from particles that are not intercepted by the lead collimator and scatter from the cylindrical cell walls. Prior to scattering, these particles travel approximately parallel to the cell’s axis through the walls (≈ 4 cm in length, Fig. 3). These particles lose a lot of energy as they pass through the glass and thus both their elastic and inelastic peaks are smeared into a very broad distribution. A software cut on the interior of the cell eliminated most events, but this cut could not eliminate events from the beam halo hitting the side walls.

Figures 7 and 8 illustrate the difference in the two background contributions from an empty cell at $T_{\pi^+}=256$ MeV and $\theta_{lab}=50^\circ$. Figure 7 is an $XYTYT$ spectrum for the empty cell. Indicated by solid lines are two software cuts, one on the upstream end cap of the target cell (where the pion beam enters) and the other on the interior region of the empty cell.

The upper panel of Fig. 8 shows the energy spectrum generated with a software cut on the upstream end cap, highlighting scattering from the thin glass windows. At this en-

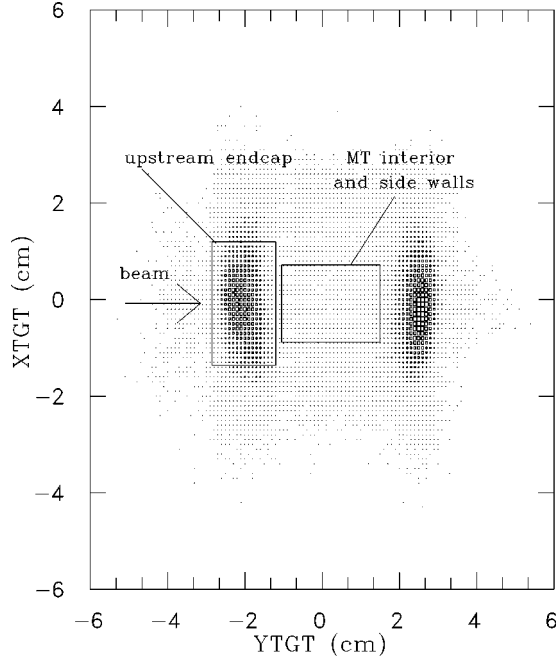


FIG. 7. $XTYT$ spectra for the evacuated target cell at $T_{\pi^+}=256$ MeV and $\theta_{lab}=50^\circ$. Indicated are the locations of software cuts on the upstream end cap of the target cell (where the pion beam enters) and on the interior region of the cell. Scattering events from the interior region of this empty cell are due to particles not intercepted by the collimator interacting with the sidewalls of the target.

ergy and angle ($T_{\pi^+}=256$ MeV and $\theta_{lab}=50^\circ$) the events from the scattering from glass, Si (g.s. and first 2^+) and O (g.s.), form one broad unresolved peak near $E_x=-14$ MeV. The large width of this peak results from the poor energy resolution and the kinematic broadening of peaks not resulting from scattering on ^3He . Similarly, events from the excitation of the $J^\pi=3^-$ states in Si and O are seen as one broad peak near -8 MeV.

The lower panel of Fig. 8 presents a spectrum generated with a software cut on the ‘‘interior region,’’ highlighting scattering from the thicker sidewalls of the empty target cell. As mentioned above, energy straggling and the large differences in energy losses before and after scattering smear out the elastic and inelastic peaks so that the events from the $XTYT$ software cut on the interior of the ^3He cell gives a glass background that varies smoothly with E_x . These background spectra M_{bck} were subtracted from the full-cell spectra.

It was not possible to take empty-cell runs at all angles for E1267 due to time constraints. However, empty-cell spectra were measured at all forward angles ($\theta_{lab}\leq 70^\circ$). Good background information was needed at these angles for two reasons. First, the effective length of the target cell L as seen by the LAS spectrometer, decreases from a maximum at 90° with decreasing laboratory angle (see Fig. 3), making it hard to distinguish the end caps from the interior of the cell. Second, at forward angles, the inelastic peak from excitations of the $J^\pi=3^-$ states in silicon and oxygen are close to the position of the ^3He elastic peak so that they could not be separated from the ^3He peak. Empty-cell spectra taken at a couple of the larger angles showed that at these angles the background had no structure near $E_x=0$ and could be fit with

a smooth polynomial shape (see Sec. IV D). Such smooth background was assumed and fitted to the spectra at the angles where no empty-cell data had been taken.

C. Asymmetries

The experimental A_y were calculated using the equation

$$A_y = \frac{C_\uparrow N_\uparrow - C_\downarrow N_\downarrow}{P(C_\uparrow N_\uparrow + C_\downarrow N_\downarrow)}, \quad (12)$$

where the relative cross sections are expressed as a product of the number of spin-sorted scattering events C_\uparrow, C_\downarrow and the normalization factors N_\uparrow, N_\downarrow . The normalizations are inversely proportional to the integrated pion beam current, measured with the beam ion chamber and proportional to a correction factor which accounts for computer live time and chamber efficiencies. In this experiment there was no loss of polarization when the sign of the polarization was changed, hence $P_\uparrow = P_\downarrow = P$.

If large backgrounds exist it is advantageous to create new histograms M_Σ and M_Δ , from the experimental spectra M_\uparrow, M_\downarrow , and M_{bck} , before fitting the peaks of interest. We define summed spectra by

$$M_\Sigma = M_\uparrow N_\uparrow + M_\downarrow N_\downarrow - 2M_{bck} N_{bck}, \quad (13)$$

where $M_{bck} N_{bck}$ is the normalized background spectrum from the empty cell runs, and difference spectra by

$$M_\Delta = M_\uparrow N_\uparrow - M_\downarrow N_\downarrow. \quad (14)$$

Note that, within statistical uncertainties, the background subtracts out when creating M_Δ , but needs to be subtracted explicitly when creating M_Σ . The summed and difference yields for elastic scattering from ^3He were then obtained by fitting the elastic peak in the properly normalized summed and difference spectra.

D. Fitting the spectra

The program NEWFIT [29] was used to generate and fit the histograms M_Σ and M_Δ defined in Eqs. (13) and (14) with a Gaussian peak near $E_x=0$ MeV and a smoothly varying background. Backgrounds arose from the ^3He breakup continuum and any events from scattering on the glass either from an incomplete background subtraction or in the cases where no empty-cell spectra had been taken. The centroid, width, and area of the Gaussian were free to vary, as were the parameters of the background that was fit with a third- to fifth-order polynomial. By fitting the peak and background in M_Σ , the values of $\Sigma = C_\uparrow N_\uparrow + C_\downarrow N_\downarrow$ for use in Eq. (12), and their standard deviations for use in Eq. (15) (see Sec. IV E) were obtained.

Subsequently, the histogram M_Δ [Eq. (14)] was fit to a Gaussian peak of the same width and centroid as the peak in M_Σ and the number of counts $\Delta = C_\uparrow N_\uparrow - C_\downarrow N_\downarrow$ in the difference peak and the standard deviation σ_Δ were obtained. The method of constraining the peak in M_Δ to the parameters of the peak in M_Σ was adopted because the statistics in the M_Σ histograms were much better than in the M_Δ histograms, particularly when the A_y were small. An example of spectra fitting is given in Fig. 9, which contains π^+ data taken at 50°

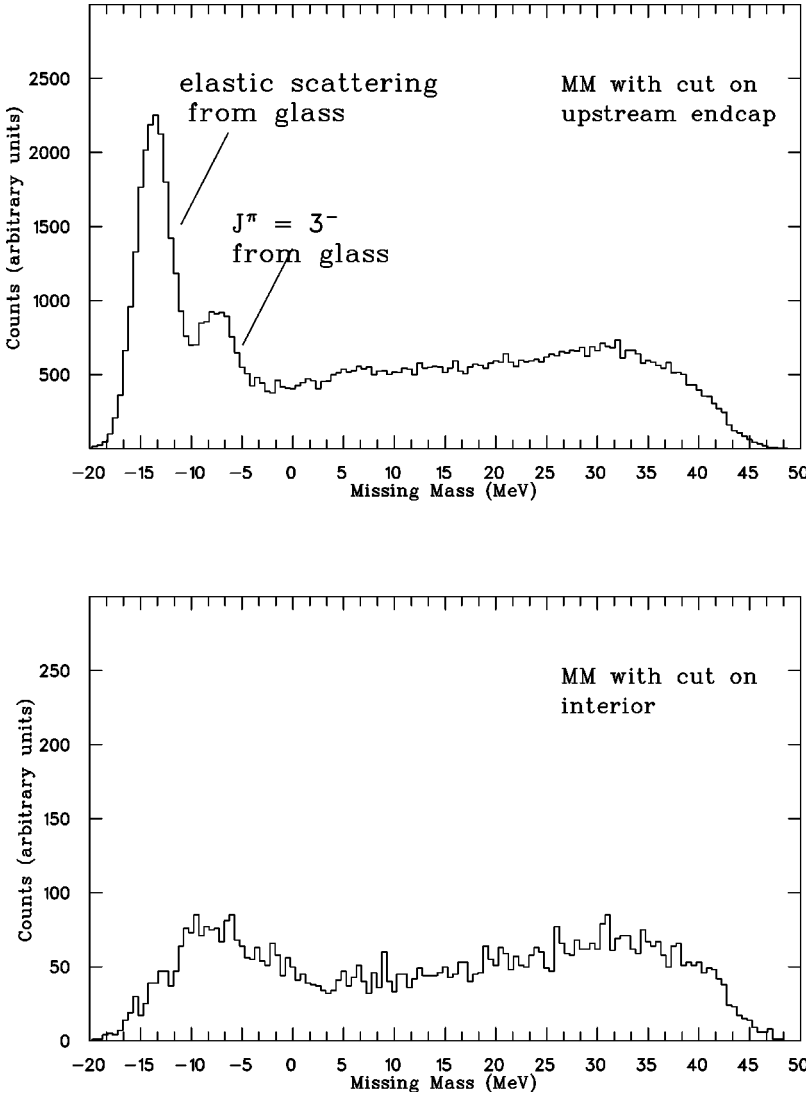


FIG. 8. Spectra from the evacuated target cell at $T_{\pi^+}=256$ MeV and $\theta_{lab}=50^\circ$. Upper panel, spectra generated with a software cut on the upstream end cap as shown in Fig. 7. Scatterings occur on the thin glass windows. The elastic events from glass (Si and O) are seen in one peak near -14 MeV; also any contribution from the $J^\pi=2^+$ state in Si would be unresolved from this peak. The $J^\pi=3^-$ states in O and Si are seen as one peak near -8 MeV. Lower panel, spectra generated with a software cut on the interior region as shown in Fig. 7. Scatterings occur in the walls of the target cell.

at 180 MeV. The upper panel of Fig. 9 shows the normalized background spectrum. The middle and lower panels of Fig. 9 show the M_Σ and M_Δ spectra. There is a large negative asymmetry indicated at $E_x=0$ and the asymmetry in the region above breakup threshold $E_x \geq 7.72$ MeV is consistent with zero.

The extracted values of A_y for elastic scattering and their uncertainties are presented in Table I and in Figs. 10, 13, and 15. The uncertainties are discussed in the next subsection.

E. Uncertainty in A_y

The uncertainties in A_y [Eq. (15)] are given by [30]

$$\sigma_{A_y}^2 = \frac{P^2(\Delta^2\sigma_\Sigma^2 + \Sigma^2\sigma_\Delta^2) + \Delta^2\Sigma^2\sigma_P^2 - 2\Sigma\Delta P^2\sigma_{\Sigma\Delta}^2}{P^4\Sigma^4}, \quad (15)$$

where σ_Σ and σ_Δ are the standard deviations of Σ and Δ . They contain contributions from uncertainties in the fitting procedure, normalization, and statistics. The $\sigma_{\Sigma\Delta}^2$ covariance term arises because Δ and Σ are determined from the independent measurements of M_\uparrow and M_\downarrow . The two major fac-

tors leading to the uncertainty in the polarization σ_P are the loss of pressure throughout the experiment and the calibration of the NMR signal by use of a water-filled cell. We estimated σ_P/P to be $\leq 10\%$ from both of these factors.

During the analysis of the E1267 data it appeared that some of the forward angle M_Δ spectra ($T_{\pi^+}=256$ MeV for $\theta_{lab}=40^\circ$ and 50° and $T_{\pi^+}=142$ MeV for $\theta_{lab}=40^\circ$ and 50°) had small asymmetries at E_x where scattering from glass was important. (There were no such asymmetries in any of the M_Δ spectra at 180 MeV for π^+ or π^- .) Such a systematic asymmetry may be the result of a slight deflection in beam position between the spin-up and spin-down states due to the reversal of the 3-mT holding field of the Helmholtz coils. This reversal causes a net deflection of the pion beam, which we estimated to be ≈ 3 mm at the target. As the beam intensity varies rapidly at the edge of the beam, a small deflection can cause a large change in the flux impinging on the glass walls. However, the yield from the glass in the region of the elastic peak from scattering on ^3He was small compared to the yields at E_x where the small asymmetries from glass appeared. Thus it was determined that any asymmetry in the background due to glass had a negligible effect on the region of the elastic scattering peak and thus on the asymmetries for ^3He .

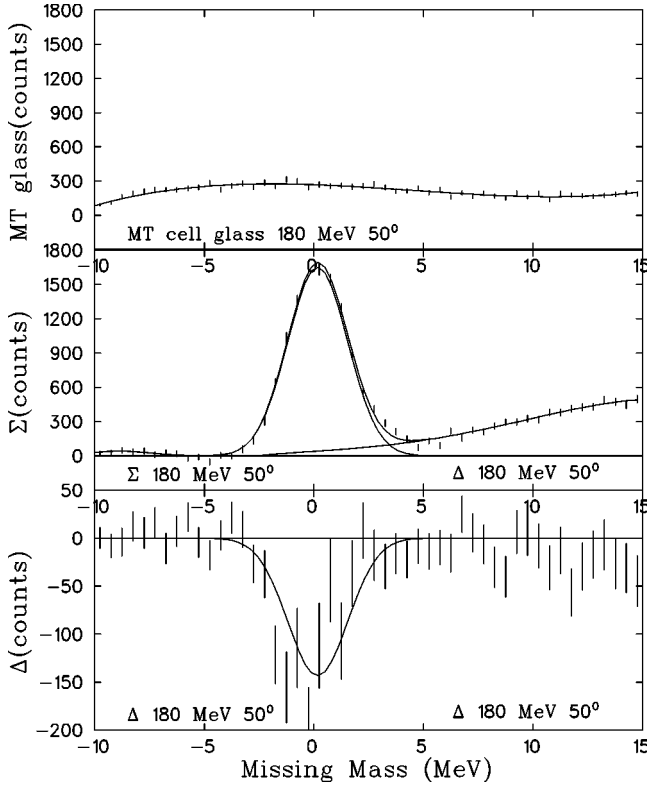


FIG. 9. Typical energy spectra for π^+ scattering measured at 180 MeV and 50° . Upper panel, normalized background spectrum; middle panel, M_Σ , normalized summed spectrum after background subtraction; bottom panel, M_Δ , difference spectrum.

V. THEORETICAL ANALYSIS AND DISCUSSION

A. Conventional models

Figure 10 presents the experimental angular distribution of A_y and predictions with the KTB model (solid lines) and the toy model (dotted lines) described earlier. The upper three panels contain the results for π^+ scattering at the three energies and the lower panel the results for π^- scattering at 180 MeV.

TABLE I. Experimental A_y for π^+ and π^- scattering from ^3He .

$T_{\pi^+}=142$ MeV		$T_{\pi^+}=180$ MeV	
θ_{lab} (deg)	A_y	θ_{lab} (deg)	A_y
40.0	-0.19 ± 0.05	40.0	-0.14 ± 0.05
50.0	-0.23 ± 0.05	50.0	-0.28 ± 0.04
60.0	-0.17 ± 0.09	60.0	-0.26 ± 0.06
70.0	0.47 ± 0.06	70.0	0.22 ± 0.07
80.0	0.82 ± 0.10	80.0	0.97 ± 0.09
90.0	0.59 ± 0.10	90.0	0.66 ± 0.09
100.0	0.48 ± 0.08	100.0	0.60 ± 0.08
$T_{\pi^+}=256$ MeV		$T_{\pi^-}=180$ MeV	
θ_{lab} (deg)	A_y	θ_{lab} (deg)	A_y
40.0	-0.16 ± 0.06	50.0	0.29 ± 0.08
50.0	-0.29 ± 0.06	65.0	0.76 ± 0.14
60.0	-0.48 ± 0.10	80.0	0.62 ± 0.10
70.0	-0.92 ± 0.16	95.0	0.18 ± 0.10

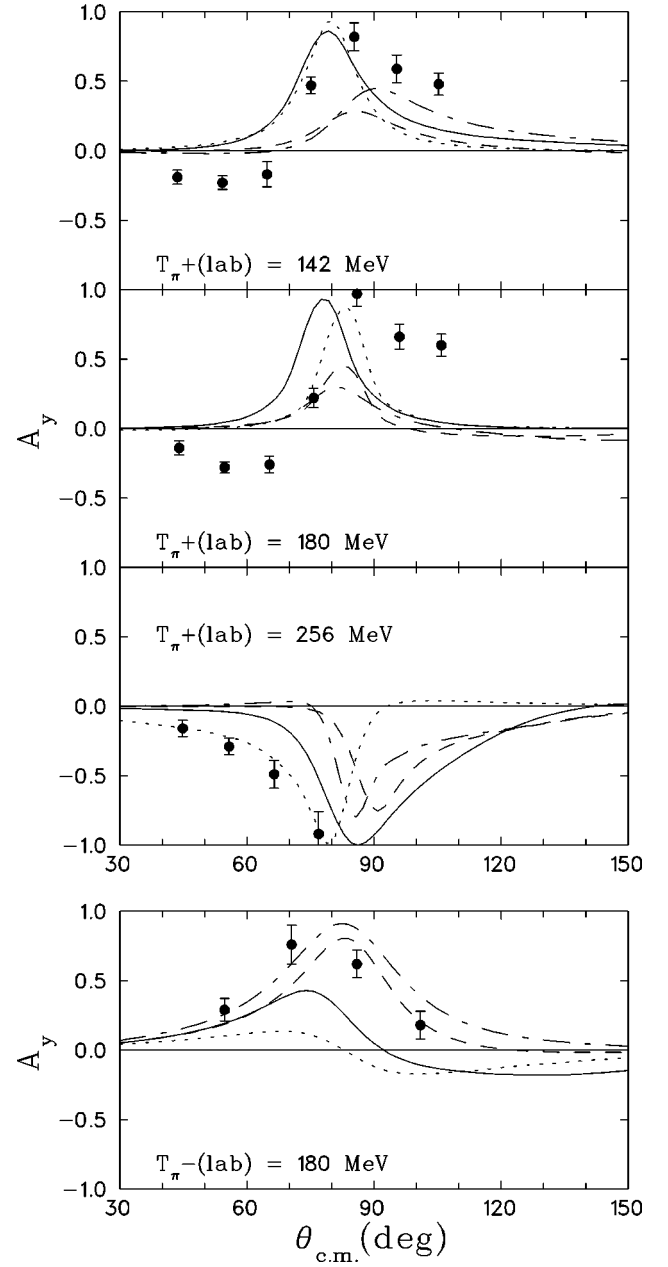


FIG. 10. Experimental and theoretical angular distribution of A_y for the elastic scattering of π^+ (upper three panels) and π^- (lower panel) from polarized ^3He . The data are from the experiments described in this paper. The solid lines are from the first-order multiple-scattering predictions of the KTB model [18]. The dotted lines are from the toy model. The dashed and chain-dashed curves are from a DWIA calculation of Ref. [20] using elementary πN amplitudes calculated with T_π at the experimental value and shifted down by 20 MeV, respectively.

In the toy model, the real part of \mathcal{F} was modified as described by Eq. (11) with $A=0, 0.2$, and 0.6 at 142, 180, and 256 MeV, respectively. These values of A are purely empirical and were chosen because by shifting the zero crossings of the real part of \mathcal{F} thus one can simulate the results of the full KTB model [18]. Also shown in this figure are the distorted-wave impulse approximation (DWIA) calculations of one of us (W.R.G.), which use the Faddeev formalism to describe the ^3He wave function. One of the DWIA calculations was done with an energy shift of 20 MeV, that is, the energy at

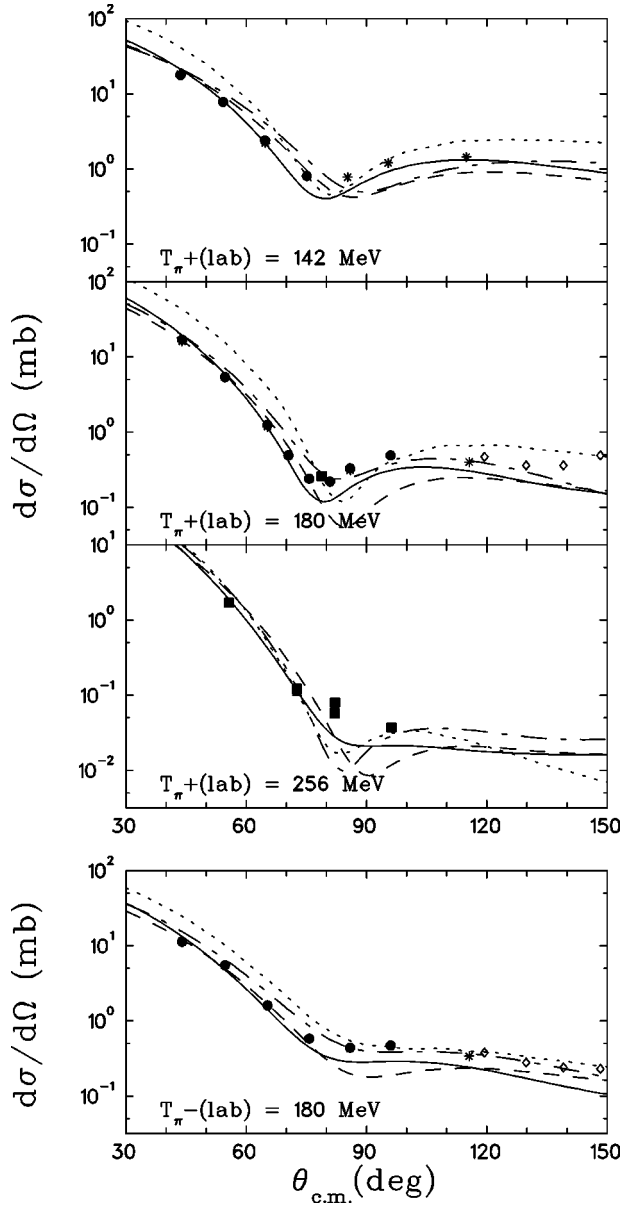


FIG. 11. Theoretical angular distributions of $d\sigma/d\Omega$ for the elastic scattering of π^+ (upper three panels) and π^- (lower panel) from polarized ${}^3\text{He}$. The curves are as in Fig. 10. The data are from Ref. [33] (black circles), Ref. [34] (asterisks), and Ref. [35] (open diamonds and black squares).

which the elementary πN amplitudes were obtained from the fitted phase shifts [23] was taken 20 MeV below the actual incident pion energy. This energy shift is often treated as an adjustable parameter and accounts in part for binding energy and Fermi motion effects [31]. The authors of Ref. [32] justify the use of an energy shift by the Δ -hole interaction. The dashed (chain-dashed) lines are from the calculations without (with) the shift of 20 MeV. None of the models give a satisfactory description of the A_y for π^+ scattering at 142 and 180 MeV, nor do the multiple-scattering calculations of Ref. [19] (not shown), which are quite similar to the calculations with the KTB model (solid lines).

The calculations completely miss the unexpected negative asymmetries at scattering angles near 60° at $T_\pi=142$ and 180 MeV. All conventional model calculations predict posi-

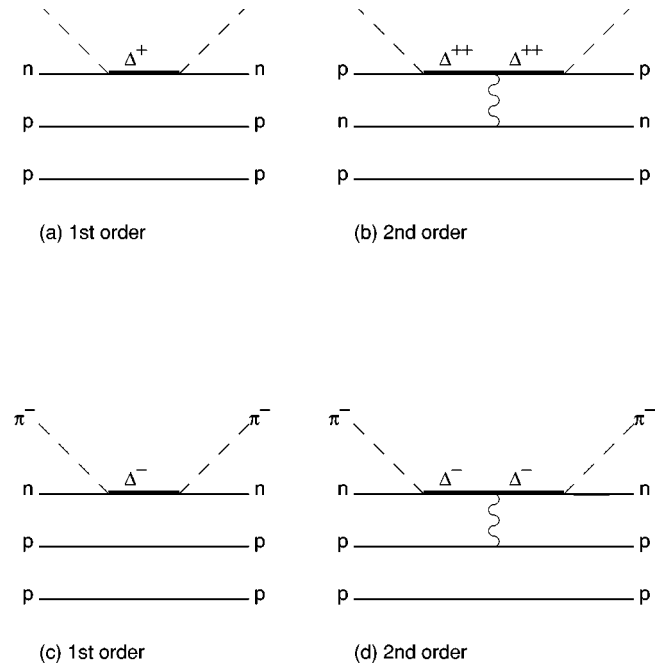


FIG. 12. Feynman diagram of first- and second-order contributions to \mathcal{G} in elastic ${}^3\text{He}(\pi,\pi)$ scattering. (a) and (b) show the contributions for π^+ . The factor of 3 in isospin coupling for π^+p over π^+n leaves the second-order term significant relative to the first-order term. (c) and (d) show the contributions for π^- . Isospin coupling is the same (π^-n) for the first- and second-order terms, thus (d) is relatively smaller than the first-order term. The wavy lines in (b) and (d) indicate the exchange of neutral π , ρ , ω , and η mesons.

tive A_y between 100 and 180 MeV at these angles. At the two energies, 142 and 180 MeV, the experimental A_y are large and positive near 80° as predicted by the multiple-scattering and toy model calculations, but the maximum of the experimental A_y is observed at larger angles than predicted. We note that the DWIA curves of W.R.G. are too low in magnitude.

The experimental A_y at 256 MeV are negative at all angles. Thus the energy at which the A_y near 80° flips from positive to negative, lies between 180 and 256 MeV. All models predict negative A_y for π^+ at 256 MeV. Only the toy model, with $\text{Re}\mathcal{F}$ modified as in Eq. (11), provides a reasonable fit, and this might well be coincidental. For the π^- data at 180 MeV, both of the DWIA predictions are closer to the data in magnitude than the KTB and toy models. The maximum of the experimental A_y is seen at a smaller angle, $\approx 70^\circ$, than predicted by any of the theoretical models.

Figure 11 shows the differential cross-section predictions for the theoretical models discussed above, as well as some of the existing data [33–35]. Except in the minima, the differential cross sections are fit quite well with the multiple-scattering calculations (solid lines). It is clear that the differential cross sections are less strongly model dependent than the asymmetries. The energy-shifted DWIA predictions (chain-dashed lines) provide a reasonable fit to the data at 180 MeV for both π^+ and π^- , although they predict deep minima in the π^+ cross section near 70° at 256 MeV where the data fall off gradually. The toy model prediction is generally too large at angles less than $\approx 80^\circ$ for all energies

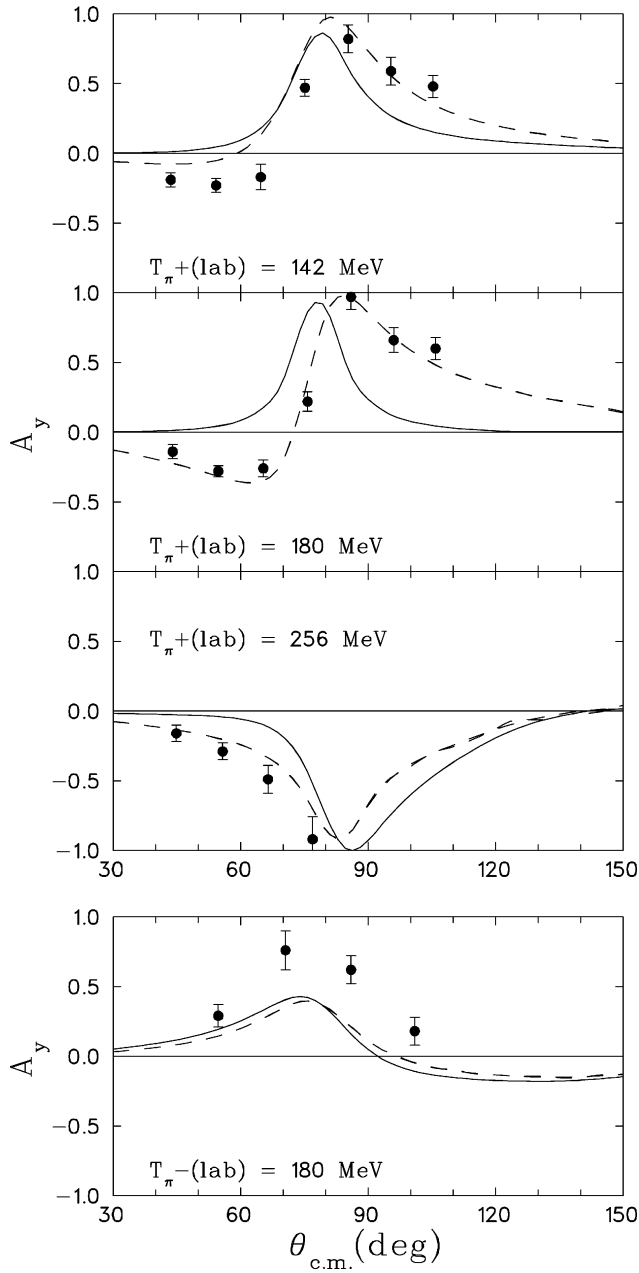


FIG. 13. Experimental and theoretical angular distribution of A_y for the elastic scattering of π^+ (upper three panels) and π^- (lower panel) from polarized ^3He . The data are from the experiments described in this paper. The solid lines are from the first-order KTB multiple-scattering model. The dashed lines are from the hybrid model, which uses the amplitudes \mathcal{F} and \mathcal{G} from the KTB model but adds the DINT term to \mathcal{G} to account for the Δ -neutron interaction.

except 256 MeV, indicating the effect of neglecting distortion effects.

B. Hybrid model

For π -nucleus scattering, large second-order effects may be caused by the Δ -nucleus interaction when the $\Delta(1232)$ resonance dominates the elementary π -nucleon interaction. (See Ref. [36] for a review of the Δ -hole model.) In this paper we specifically address the need for including a Δ -neutron spin-spin interaction in calculations of asymmetries.

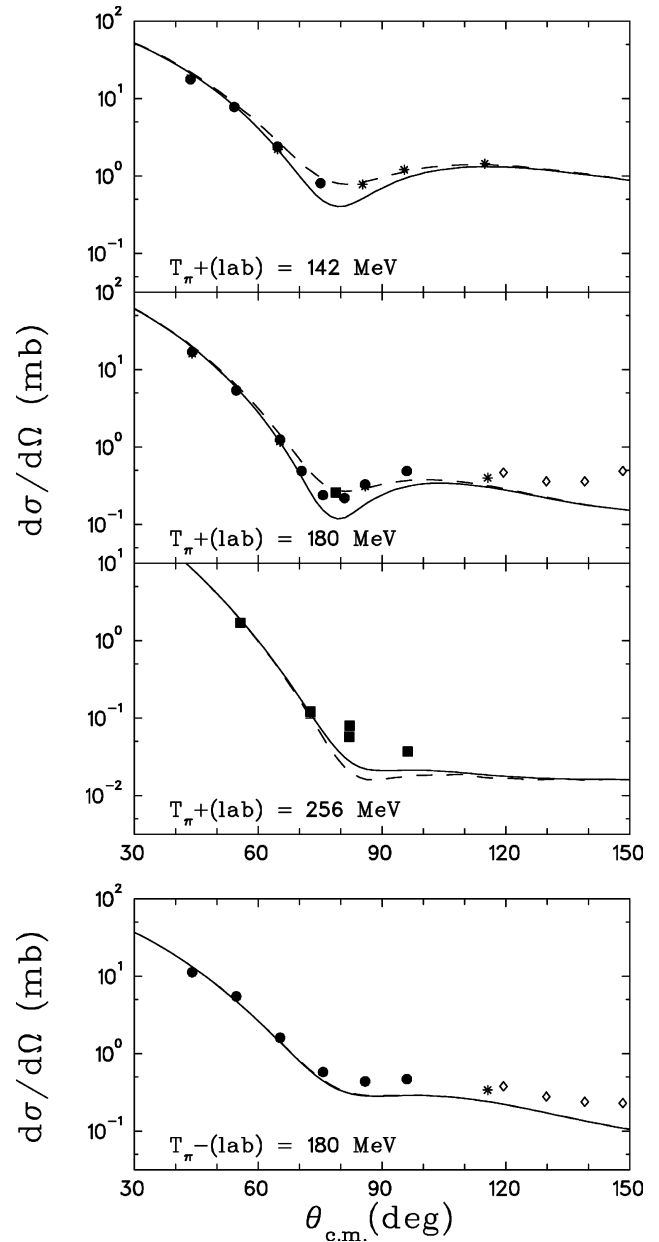


FIG. 14. Experimental and theoretical angular distributions of $d\sigma/d\Omega$ for the elastic scattering of π^+ (upper three panels) and π^- (lower panel) from polarized ^3He . The curves are as in Fig. 13 and the data are as in Fig. 11.

As pointed out above, π scattering on the paired-off protons of the fully space-symmetric part of the ground state of ^3He cannot contribute to the first-order spin-dependent amplitude \mathcal{G} . To first order, \mathcal{G} results only from scattering from the unpaired neutron, whereas \mathcal{F} has a large (first-order) component from scattering from the two protons and a small one from scattering from the neutron. However, a large second-order contribution to \mathcal{G} arises if the intermediate Δ^{++} , generated with very high probability in π^+ scattering on one of the two protons, interacts with the polarized neutron. [Recall that for the $\Delta(1232)$ resonance the π -nucleon isospin coupling Clebsch-Gordan coefficients result in much larger scattering amplitudes \mathcal{F} and \mathcal{G} for π^+ elastic scattering on protons than on neutrons leading to the ratio of 9:1 in π^+p/π^+n differential cross sections.]

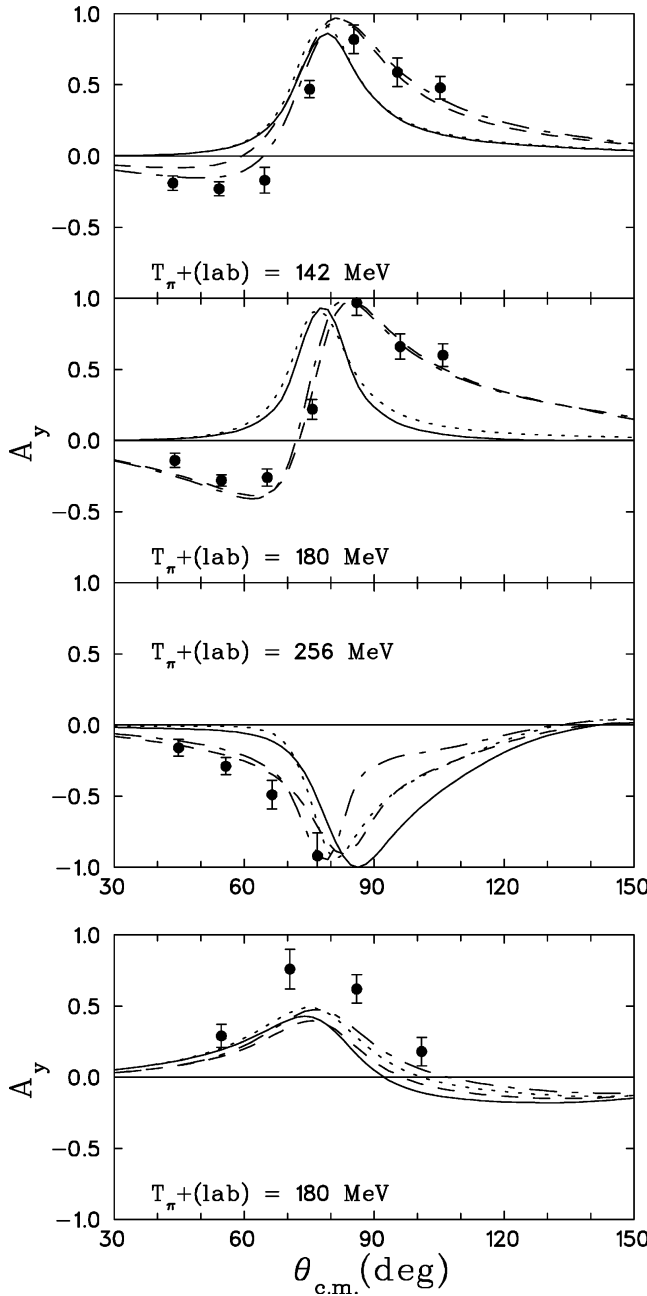


FIG. 15. Experimental and theoretical angular distribution of A_y for the elastic scattering of π^+ (upper three panels) and π^- (lower panel) from polarized ^3He . The data are from the experiments described in this paper. The solid and dashed lines are from the first-order KTB multiple-scattering predictions and hybrid model, respectively, as shown in Fig. 13. The dotted lines are from the first-order KTB multiple-scattering model with the pion KE for the elementary πN amplitudes shifted accordingly. The chain-dashed lines are from the hybrid model using the “shifted” KTB amplitudes \mathcal{F} and \mathcal{G} and adding the DINT term to \mathcal{G} to account for a second-order Δ -neutron interaction.

This is illustrated in Figs. 12(a) and 12(b), which show the first- and second-order contributions to \mathcal{G} for π^+ scattering. Although the second-order DINT contribution [Fig. 12(b)] is expected to be smaller than the first-order term [Fig. 12(a)], the higher isospin coupling factor for $\pi^+ p$ over $\pi^+ n$ scattering makes the Δ -neutron interaction term significant

relative to the first-order term. For the π^- case, the isospin coupling ($\pi^- n$) coefficient is the same large value for the first and second-order terms [Figs. 12(c) and 12(d), respectively]. Thus the contribution of the DINT term to \mathcal{G} is expected to be small relative to first-order effects in the π^- case.

The magnitude of the second-order contribution to \mathcal{G} has been investigated by one of us (B.K.J.) using the simple s -shell model for ^3He with Gaussian single-particle wave functions. The rms radius of the nucleon distribution in ^3He was kept fixed at the value $\langle r^2 \rangle^{1/2} = 1.65$ fm obtained by unfolding the finite proton size from the charge density of ^3He [37]. This model employs the plane-wave impulse approximation for the second-order term and a meson exchange model for the Δ -neutron interaction, which includes the neutral π , ρ , ω , and η mesons. Meson exchange is indicated by the wavy lines in Figs. 12(b) and 12(d). The meson- Δ couplings were obtained from the meson-nucleon couplings by use of SU(6) symmetry and the naive quark model. Two-nucleon correlations were included phenomenologically by multiplying the wave function with a Gaussian correlation function that depends on the relative distance of the interacting particles. The width of the correlation Gaussian was kept fixed at a standard value of 0.75 fm [38]. The resulting second-order term in \mathcal{G} was added to the first-order multiple-scattering values for \mathcal{F} and \mathcal{G} obtained in the KTB model.

The results of this “hybrid model” calculation are shown in Fig. 13 (dashed lines) along with the predictions of the KTB model shown before (solid lines). The curves for π^+ were obtained by fixing the π and η meson- Δ couplings at the SU(6) values (see Ref. [39]) and performing a search on the strengths of the ρ - Δ and ω - Δ couplings. It was found that a best fit to the asymmetry data occurs when these couplings differ by roughly 20–30% from their SU(6) values of Ref. [39], which is within the commonly accepted value for SU(3) symmetry breaking. For the π^- data, the meson- Δ couplings were held at the SU(6) value.

The hybrid model gives an improved fit to all the π^+ data. At 180 MeV the negative A_y near 60° and the shift of the positive maximum towards larger angles are reproduced. At 142 MeV, the magnitude of the negative A_y near 60° is not described as well, but is in better agreement with the data than the KTB model. At 256 MeV, the model including the DINT term is again in better agreement with the data than the multiple-scattering calculation without it.

The hybrid model is not much different from the KTB model in the case of the π^- data. This is expected since the relative amplitude of the (second-order) DINT term is small compared to the first-order term (Fig. 12). However, the KTB model predicts values of A_y too small in amplitude and so does the hybrid model.

The effect of the $\Delta^{++}n$ interaction on the differential cross sections is shown in Fig. 14. For π^+ scattering, the DINT term fills in the minima at 142 and 180 MeV, resulting in improved fits. The DINT term slightly worsens the fit in the minimum at 256 MeV. It has a very small effect on the π^- cross section at 180 MeV, again as expected.

C. Hybrid model predictions with energy shifts

As mentioned above, shifting the kinetic energy at which the elementary πN amplitudes are calculated ≈ 20 MeV

lower than the actual incident energy can improve the description of the cross-section data in this energy region. For example, Ref. [40] obtained the best fit to elastic ${}^4\text{He}(\pi, \pi)$ scattering data by optical model calculations that use elementary πN amplitudes obtained with the energy shifted down by $\Delta E = (T_\pi + 10 \text{ MeV})/10$ for pion energies below 170 MeV and a constant value of 18 MeV for higher energies. This prescription is consistent with fits to data on a variety of nuclei [41].

One of us (S.S.K.) calculated ‘‘shifted’’ KTB amplitudes using $\Delta E = 15 \text{ MeV}$ for 142 MeV and $\Delta E = 20 \text{ MeV}$ at 180 and 256 MeV. Figure 15 shows the experimental A_y and the predictions with the shifted KTB amplitudes (dotted lines). The hybrid model (chain-dashed lines) with energy shift uses the amplitudes \mathcal{F} and \mathcal{G} from the KTB model with the energy-shifted πN amplitudes and adds the term for the Δ -neutron interaction. Also shown for reference are the predictions of Sec. V B for the KTB (solid lines) and hybrid models (dashed lines) obtained without the energy-shifted amplitudes.

The dotted curves for the π^+ data were obtained with the shifted KTB model and the chain-dashed curves were obtained in the shifted hybrid model with a new search on the meson- Δ coupling strengths. The π and η meson- Δ couplings were held fixed at the SU(6) values and the strengths of the ρ - Δ and ω - Δ couplings were allowed to vary, as described in Sec. V B. The best fit to the data was attained with these couplings being very similar to those of the previous calculation.

Without DINT, neither the unshifted (solid lines) nor the shifted (dotted lines) KTB model can explain the negative A_y at angles near 60° in the π^+ data. The shifted KTB model for π^- scattering gives larger A_y than the unshifted prediction, but still too small values compared to experiment.

The hybrid model with the energy-shifted KTB amplitudes (chain-dashed lines) does a better job than the hybrid model without the shift (dashed lines) in describing the π^+ data at 142 MeV. At 180 and 256 MeV, the effect of the energy shift on A_y is quite small so that the good fits obtained without the energy shift are maintained.

The predictions for the differential cross sections are shown in Fig. 16. At 142 MeV, the DINT term (in both the shifted and unshifted models) fills in the minimum of the cross section for a better fit to the data. At 180 MeV (π^+) the KTB model with the energy shift provides the best fit to the data. Including a DINT term fills in the minima a bit too much. At 256 MeV, all models predict a minimum which is not seen in the data. For the π^- cross section, the KTB and hybrid models are similar in both the shifted and unshifted cases, with the energy shift providing the better description of the data. With the combination of the DINT term and the energy shift in the elementary πN amplitudes, it appears that both the A_y and cross-section data are fit much better than with the conventional models.

The need of including a Δ -nucleon interaction has been invoked previously in an analysis [42] of vector analyzing powers from $\pi^- \vec{d}$ scattering [43,44]. The $\pi^- \vec{d}$ scattering analysis added the Δ - N interaction in the Born term only to background few-body amplitudes. Later theoretical work [45,46] that included DINT to all orders found that higher-

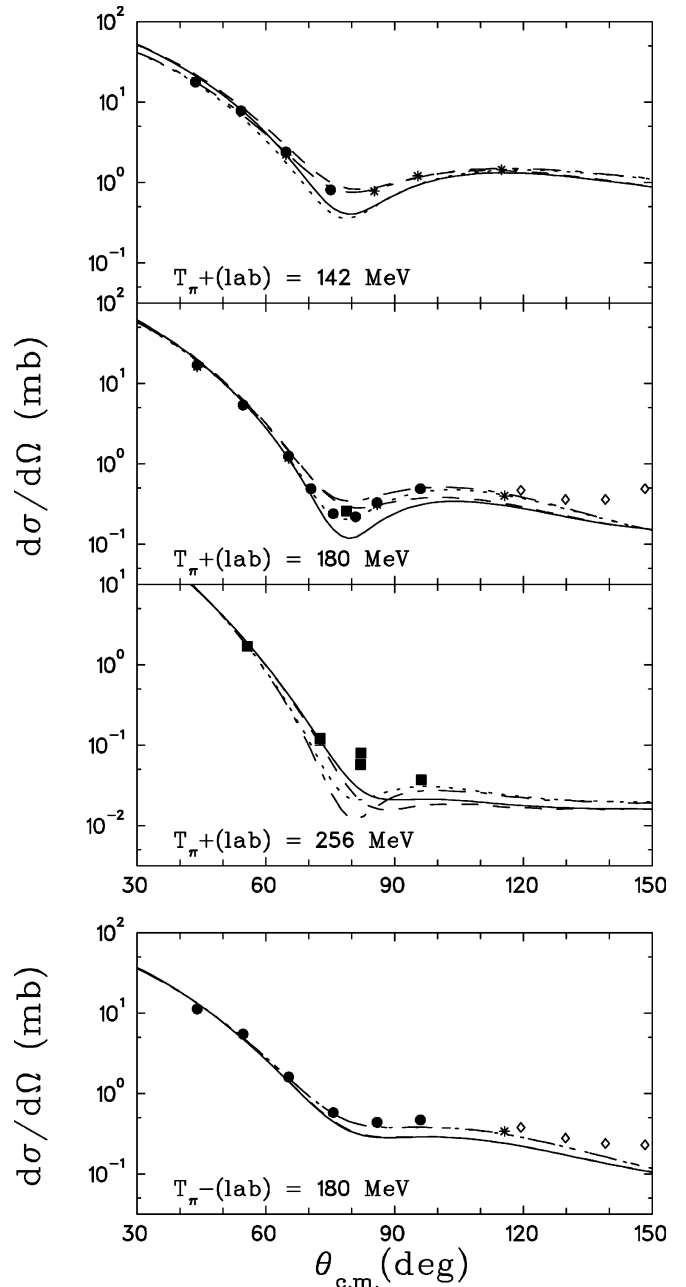


FIG. 16. Experimental and theoretical angular distributions of $d\sigma/d\Omega$ for the elastic scattering of π^+ (upper three panels) and π^- (lower panel) from polarized ${}^3\text{He}$. The curves were calculated as for Fig. 15 and the data are the same as in Fig. 11.

order DINT terms tend to cancel the effects obtained by the adding the Δ - N Born term. Thus the discrepancies between theoretical and experimental vector analyzing powers for $\pi^- \vec{d}$ are still unexplained. We note that a recent study of π^+ photoproduction on ${}^3\text{He}$ [47] found that the inclusion of the DINT mechanism was important.

VI. CONCLUDING REMARKS

Further theoretical work is needed to determine whether our measured A_y can be explained by some aspect of the reaction mechanism or the ${}^3\text{He}$ wave function, which we

have not yet included. In light of what has been learned from the theoretical analysis of the $\pi\vec{d}$ data, it is especially important that the Δ - N interaction be treated as part of the full multiple-scattering calculations and not simply added on as in our model. Also, the effects of pion absorption and the Δ - N spin-orbit interaction need to be investigated. This paper and a previous Letter [1] present an attempt to treat the Δ - N interaction in π - $^3\overline{\text{He}}$ scattering microscopically.

ACKNOWLEDGMENTS

The authors wish to thank Yin Tan for her help in taking the data. The authors are also indebted to Dr. R. L. Boudrie and the technical staff at LAMPF for their help and support. This work was supported in part by the U.S. Department of Energy, the National Science Foundation, the Natural Sciences and Engineering Research Council of Canada, and the Graduate School of the University of Minnesota.

-
- [1] M. A. Espy *et al.*, Phys. Rev. Lett. **76**, 3667 (1996).
 [2] See, for example, Los Alamos National Laboratory Report No. LA-10772-C, 1986 (unpublished).
 [3] R. Tacik *et al.*, Phys. Rev. Lett. **63**, 1784 (1989).
 [4] R. Meier *et al.*, Phys. Rev. C **50**, 2222 (1990).
 [5] Yi-Fen Yen *et al.*, Phys. Rev. Lett. **66**, 1959 (1991).
 [6] Yi-Fen Yen, Ph.D. thesis, University of Minnesota, 1991 (unpublished).
 [7] Yi-Fen Yen *et al.*, Phys. Rev. C **50**, 897 (1994).
 [8] J. T. Brack *et al.*, Phys. Rev. C **45**, 698 (1992).
 [9] R. Mach and S. S. Kamalov, Nucl. Phys. **A511**, 601 (1990).
 [10] S. Chakravarti *et al.*, Univeristy of Minnesota Report No. COO-87ER40362-3, 1990 (unpublished); D. Dehnhard *et al.*, Few-Body Syst. Suppl. **5**, 274 (1992).
 [11] P. B. Siegel and W. R. Gibbs, Phys. Rev. C **48**, 1939 (1993), and private communication.
 [12] R. A. Brandenburg, Y. E. Kim, and A. Tubis, Phys. Rev. C **12**, 1368 (1975).
 [13] J. L. Friar *et al.*, Phys. Rev. C **34**, 1463 (1986).
 [14] D. R. Tilley, H. R. Weller, and H. H. Hasan, Nucl. Phys. **A474**, 2 (1987).
 [15] Bart W. Larson, Ph.D. thesis, Simon Fraser University, 1991 (unpublished); B. Larson *et al.*, Phys. Rev. A **44**, 3108 (1991).
 [16] B. Larson *et al.*, Phys. Rev. Lett. **67**, 3356 (1991).
 [17] B. Larson *et al.*, Phys. Rev. C **49**, 2045 (1994).
 [18] S. S. Kamalov, L. Tiator, and C. Bennhold, Phys. Rev. C **47**, 941 (1993); C. Bennhold, B. K. Jennings, L. Tiator, and S. S. Kamalov, Nucl. Phys. **A540**, 621 (1992).
 [19] S. Chakravarti, C. M. Edwards, D. Dehnhard, and M. A. Franey, Few-Body Syst. Suppl. **5**, 267 (1992).
 [20] W. R. Gibbs (private communication).
 [21] J. M. O'Donnell *et al.*, 1996 APS Spring Meeting in Indianapolis [Bull. Am. Phys. Soc. **41**, 878 (1996)].
 [22] R. J. Cence, *Pion-Nucleon Scattering* (Princeton University Press, Princeton, 1969).
 [23] R. A. Arndt *et al.*, The SAID program: A Guide to Users (unpublished).
 [24] A. K. Kerman, H. McManus, and R. M. Thaler, Ann. Phys. (N.Y.) **8**, 551 (1959).
 [25] W. J. Cummings *et al.*, Phys. Rev. A **51**, 4842 (1995).
 [26] E. Coltun, Nucl. Instrum. Methods **178**, 95 (1980).
 [27] Allen L. Williams, Ph.D. thesis, University of Texas at Austin, 1991 (unpublished).
 [28] L. G. Atencio, J. F. Amann, R. L. Boudrie and C. L. Morris, Nucl. Instrum. Methods **187**, 381 (1981).
 [29] C. Morris, program NEWFIT (private communication).
 [30] J. M. O'Donnell (unpublished).
 [31] R. H. Landau and A. W. Thomas, Nucl. Phys. **A302**, 461 (1978); R. Mach and M. G. Sapozhnikov, J. Phys. G **10**, 147 (1984).
 [32] M. B. Johnson and D. J. Ernst, Ann. Phys. (N.Y.) **219**, 266 (1992).
 [33] B. M. K. Nefkens *et al.*, Phys. Rev. C **41**, 2770 (1990).
 [34] C. Pillai *et al.*, Phys. Rev. C **43**, 1838 (1991).
 [35] S. K. Mathews *et al.*, Phys. Rev. C **51**, 2534 (1995).
 [36] T. Ericson and W. Weise, *Pions and Nuclei* (Clarendon, Oxford, 1988), p. 238.
 [37] H. De Vries, C. W. De Jager, and C. De Vries, At. Data Nucl. Data Tables **36**, 495 (1987).
 [38] B. H. J. McKellar and B. F. Gibson, Phys. Rev. C **30**, 322 (1984).
 [39] R. Machleidt, Adv. Nucl. Phys. **19**, 189 (1989).
 [40] B. Brinkmüller *et al.*, Phys. Rev. C **44**, 2031 (1991).
 [41] W. R. Cottingham and D. B. Holtkamp, Phys. Rev. Lett. **45**, 1828 (1980).
 [42] E. Ferreira and H. G. Dosch, Phys. Rev. C **40**, 1750 (1989).
 [43] E. L. Mathie *et al.*, Phys. Rev. C **41**, 193 (1990).
 [44] W. List *et al.*, Phys. Rev. C **37**, 1587 (1988).
 [45] C. Alexandrou and B. Blankleider, Phys. Rev. C **42**, 517 (1990).
 [46] H. Garcilazo, Phys. Rev. C **42**, 2334 (1990).
 [47] J. A. Gómez Tejedor, S. S. Kamalov, and E. Oset, Phys. Rev. C **54**, 3160 (1996).